# A Novel Route for Synthesizing Silica Nanotubes with Chiral Mesoporous Wall Structures

Xiaowei Wu,[†] Juanfang Ruan,[‡] Tetsu Ohsuna,[§] Osamu Terasaki,[‡] and Shunai Che*[,†]

*School of Chemistry and Chemical Technology, State Key Laboratory of Composite Materials, Shanghai Jiao Tong University, Dongchuan Road 800, Shanghai 200240, People's Republic of China, Structural Chemistry, Arrhenius Laboratory, Stockholm University, S-10691 Stockholm, Sweden, and CREST, Japan Science and Technology Agency, Honcho 4-1-8, Kawaguchi-shi, Saitama, 332-0012, Japan*

*Received October 4, 2006. Revised Manuscript Received December 14, 2006*

Right- and left-handed excess chiral mesoporous silica nanotubes with a helical channel in the wall have been formed by the self-assembly of an achiral surfactant sodium dodecyl sulfate (SDS) in the presence of (*R*)-(+)- and (*S*)-(−)- 2-amino-3-phenyl-1-propanol ((*R*)-(+)- and (*S*)-(−)-APP) chiral molecules. Transmission electron microscopy combined with computer simulations confirmed the presence of ordered chiral channels winding around the central axis of the tubes of ∼100 nm inner diameter. Furthermore, it has been found that these have been produced through a specific crystallization route that hollows out the chiral mesoporous silica rod, which is different from the tube synthesis pathways reported previously. The enantiomeric excess ee of chiral mesoporous silica has been increased from 0 to a maximum value of 32% with increasing (*R*)-(+)-APP/SDS molar ratios from 0 to 0.8.

## Introduction

Tubular architectures with a nanometer-sized hollow cavity have attracted increasing attention in natural science and materials science fields from the viewpoint of their potential applications and the continuing interest in fundamental phenomena specific to a confined nanospace.[1−6] Hierarchical materials containing both interconnected macroporous and mesoporous structures have enhanced properties compared with single-sized pore materials due to increased capabilities of mass transport through the material and maintenance of a specific surface area on the level of fine pore systems.[7−12] Mesostructured nanotubes are very interesting from three different kinds of surfaces; the outer surface, the inner surface of the central tubular cavity, and the internal surface of the tubule sheath, which consists of the mesopores.[9a] The silica nanotubes with chiral mesostructure in the wall and the chiral mesoporous silica with a macrosized hollow will be the most interesting, because they may be used in the fields of chiral selectivity, chiral recognition, and chiral catalysis.

Since the first report on the synthesis of MCM-41 type hollow tubules in a high alkaline solution by Mou's group,[12a] a few mesostructured silica tubules have been prepared by means of soft templates such as surfactant[9] and long-chain alkylsilane.[11] Different kinds of helical tubular structures have been found, i.e., single-strand helical nanotubes, double-helical nanotubes, helical bundles,[13,14] and innerhelical structure[15] by a sol−gel transcription process. Typically, it has been considered that rod-shaped molecular assemblies can produce tubular morphologies of silica, or the morphology of a helical fiber could turn out to be helical tubes, respectively. Furthermore, Wu et al. have synthesized silica mesostructures with chiral mesopores such as single- and double-helical geometries inside individual alumina nanochannels.[16]

Recently, we reported that the left-handed excess[17] and racemic[18] chiral mesoporous silica with twisted 2d-hexagonal

* To whom correspondence should be addressed. Fax: 86-21-5474-1297. Tel: 86-21-5474-2852. E-mail: chesa@sjtu.edu.cn.
† Shanghai Jiao Tong University.
‡ Stockholm University.
§ CREST.

(1) Iijima, S. *Nature* **1991**, *354*, 56.
(2) Fuhrhop, J. H.; Spiroski, D.; Boettcher, C. *J. Am. Chem. Soc.* **1993**, *115*, 1600.
(3) Schnur, J. M.; Ratna, B. R.; Selinger, J. V.; Singh, A.; Jyothi, G.; Easwaran, K. R. K. *Science* **1994**, *264*, 945.
(4) Collins, P. G.; Zettl, A.; Bando, H.; Thess, A.; Smalley, R. E. *Science* **1997**, *278*, 100.
(5) For example, see Bong, D. T.; Clark, T. D.; Granja, J. R.; Ghadiri, M. R. *Angew. Chem., Int. Ed.* **2001**, *40*, 988.
(6) Mitchison, T.; Kirshner, M. *Nature* **1984**, *312*, 232.
(7) Yang, P.; Deng, T.; Zhao, D.; Feng, P.; Pine, D.; Chmelka, B. F.; Whitesides, G. M.; Stucky, G. D. *Science* **1998**, *282*, 2244.
(8) Huang, L.; Wang, Z.; Sun, J.; Miao, L.; Li, Q.; Yan, Y.; Zhao, D. *J. Am. Chem. Soc.* **2000**, *122*, 3530.
(9) (a) Kleitz, F.; Marlow, F.; Stucky, G. D.; Schüth, F. *Chem. Mater.* **2001**, *13*, 3587. (b) Kleitz, F.; Wilczok, U.; Schüth, F.; Marlow, F. *Phys. Chem. Chem. Phys.* **2001**, *3*, 3486. (c) Marlow, F.; Kleitz, F. *Microporous Mesoporous Mater.* **2001**, *44*, 671. (d) Yang, S. M.; Sokolov, I.; Coombs, N.; Kresge, C. T.; Ozin, G. A. *Adv. Mater.* **1999**, *11*, 1427. (e) Harada, M.; Adachi, M. *Adv. Mater*, **2000**, *12*, 839. (f) Adachi, M.; Harada, T.; Harada, M. *Langmuir* **2000**, *16*, 2376.
(10) Yuan, Z.; Su, B. *J. Mater. Chem.* **2006**, *16*, 663.
(11) Kim, M.; Sohn, K.; Kim, J.; Hyeon, T. *Chem. Commun.* **2003**, 652.
(12) (a) Lin, H. P.; Mou, C. Y. *Science* **1996**, *273*, 765. (b) Lin, H. P.; Mou, C. Y.; Liu, S. B. *Adv. Mater.* **2000**, *12*, 103.
(13) (a) Jung, J. H.; Ono, Y.; Hanabusa, K.; Shinkai, S. *J. Am. Chem. Soc.* **2000**, *122*, 5008. (b) Jung, J. H.; Ono, Y.; Shinkai, S. *Chem.—Eur. J.* **2000**, *6*, 4552. (c) Kobayashi, S.; Hamasaki, N.; Suzuki, M.; Kimura, M.; Shirai, H.; Hanabusa, K. *J. Am. Chem. Soc.* **2002**, *124*, 6550. (d) Jung, J. H.; Yoshida, K.; Shimizu, T. *Langmuir* **2002**, *18*, 8724. (e) Sugiyasu, K.; Tamaru, S.; Takeuchi, M.; Berthier, D.; Huc, I.; Oda, R.; Shinkai, S. *Chem. Commun.* **2002**, 1212.
(14) Seddon, A. M.; Patel, H. M.; Burkett, S. L.; Mann, S. *Angew. Chem., Int. Ed.* **2002**, *41*, 2988.
(15) Jung, J. H.; Shinkai, S.; Shimizu, T. *Chem. Mater.* **2003**, *15*, 2141.
(16) Wu, Y.; Cheng, G.; Katsov, K.; Sides, S. W.; Wang, J.; Tang, J.; Fredrickson, G. H.; Moskovits, M.; Stucky, G. D. *Nat. Mater.* **2004**, *3*, 816.

10.1021/cm062368m CCC: $37.00 
Published on Web 02/28/2007

structure could be synthesized by using chiral anionic surfactant *N*-miristoyl-L-alanine sodium salt and achiral surfactant SDS, respectively, which opened up a new approach for the synthesis of novel mesoporous materials. On the other hand, in liquid crystal science, it is well-known that the lyotropic nematic can transform into lyotropic cholesteric transitions induced by selected chiral dopants.[19] In a nature of the example, we have attempted to synthesize the chiral sense excess mesoporous silica with the introduction of one or more chiral centers in achiral surfactant SDS mesoporous synthesis system. Among the enormous chiral molecules, chiral amino alcohols have been chosen to be used as dopants with a view to the interaction between the negatively charged sulfate head group of SDS and the positively charged amino group of the amino alcohols (pKa $\approx$ 10) under the synthesis solution with a pH value of $\sim$8.5. It has been supposed that the presence of chiral amino alcohol interacts with the head group of the surfactant and induces changes in the chiral micellar direction, leading to an increase of chiral sense excess. Several amino alcohol chiral dopants such as (*R*)-(+)- and (*S*)-(−)-APP, (R)-(−)-2-amino-1-phenylethanol, l-alaninol and (S)-(+)-2-amino-3-methyl-1-butanol, etc., have been introduced into the system.

Interestingly, here we found that the increasing chiral sense excess was accompanied by the formation of mesoporous silica nanotubes with an increasing amount of dopants. Here, the influence of (*R*)-(+)- and (*S*)-(−)-APP dopant for the crystallization of the mesoporous silica nanotube has been investigated in detail with different (*R*)-(+)-APP/SDS molar ratios and the structural transformation with reaction time. The structure of chiral mesoporous silica nanotubes was analyzed by electron microscopy combined with computer simulations.

## Experimental Section

**Chemicals.** SDS (TCI), *N*-trimethoxysilylpropyl-*N*,*N*,*N*-trimethylamonium chloride (TMAPS, Azmax), tetraethyl orthosilicate (TEOS, TCI), and APP (Aldrich) were purchased and used as received.

**Synthesis of Mesoporous Silica.** The silica nanotubes with chiral wall mesostructure and chiral mesoporous silica with a macrohollow can be readily made using a one-step route according to the following procedure. Typically, the SDS and (*R*)-(+)-APP or (*S*)-(−)-APP were dissolved in sufficient water to form a clear solution, and the silica precursor, TEOS, and co-structure-directing agent (CSDA) TMAPS were then added into the clear solution at room temperature under stirring. The molar ratios of the resulting gels were 1SDS:*x*APP:0.38TMAPS:7TEOS:1680$H_2O$, where *x* was varied in the range of 0−0.8. After 5 min of stirring, the mixed solution was kept at 30 °C for 6 h and then allowed to be aged for 1 day at 90 °C. Surfactant was removed by exhaustive solid−liquid extraction overnight using HCl (1 M) in ethanol or calcination in air under 550 °C. The silica nanotubes with chiral mesostructure were produced in high yield ($\sim$99%).

**Characterization.** Powder X-ray diffraction XRD patterns were recorded on a Rigaku X-ray diffractometer D/MAX-2200/PC using Cu K$\alpha$ radiation (40 kV, 20 mA) at the rate of 1.0 ° 2$\theta$/min over the range of 1−6° 2$\theta$. The microscopic features of all samples were observed with scanning electron microscopy (SEM) (JEOLJSM-7401F). To observe genuine external surface, the samples were observed without any metal coating. An accelerating voltage, 1 kV (resolution: ca.1.4 nm) was chosen for all mesoporous silica samples. High-resolution transmission electron microscopy (HR-TEM) was performed with a JEOL JEM-3010 microscope operating at 300 kV ($C_s$ = 0.6 mm, resolution 1.7 Å). Images were recorded with a CCD camera (MultiScan model 794, Gatan, 1024 × 1024 pixels, pixel size 24 × 24 $\mu$m) at 50 000−80 000 K magnification under low-dose conditions. The nitrogen adsorption/desorption isotherms were measured at 77 K with a Quantachrome Nova 4200E porosimeter. The surface area was calculated by the Brunauer−Emmett−Teller (BET) method, and the pore size was obtained from the maxima of the pore size distribution curve calculated by the Barrett−Joyner−Halenda (BJH) method using the adsorption branch of the isotherm. Solid-state $^{13}C$ MAS NMR spectra of the mesoporous materials were collected on a Varian Mercury plus-400 NMR spectrometer.

## Results and Discussions

**1. Chiral Mesoporous Silica Nanotube with the Addition of (*R*)-(+)-APP.** The synthesis of mesoporous silica was performed using TEOS as a silica source and SDS as a surfactant under various (*R*)-(+)-APP/SDS molar ratios in the range of 0−0.8. Figures 1−4 show the SEM images, HRTEM images, XRD patterns, $N_2$ adsorption−desorption isotherms, and pore size distributions of the chiral mesoporous materials synthesized with different (*R*)-(+)-APP/SDS molar ratios at 90 °C for 1 day.

From the SEM images (Figure 1), it can be seen that all of these materials have a twisted hexagonal rodlike morphology and become hollow with increasing (*R*)-(+)-APP/SDS molar ratio. The length ranged from $\sim$1 to $\sim$4 $\mu$m and the outer diameters were $\sim$120 nm. The HRTEM image (Figure 2) with incident beam perpendicular to the rod shows ordered fringes in the same distance as that indicated by the arrows (also see Figure S1 of the Supporting Information for the low-magnification TEM image). In a manner similar to that of the samples reported previously,[17,18,20] the sample synthesized without the addition of any (*R*)-(+)-APP (Figure 2a) can be considered to be chiral mesoporous silica with highly ordered 2d-hexagonal chiral channels running inside, winding around the central axis of the solid rod. Interestingly, the chiral mesoporous materials were gradually changed from the solid rod to the macroporous hollow tube (images b and c of Figure 2), the complete hollow helical tube has been formed when a (*R*)-(+)-APP/SDS molar ratio of 0.6−0.8 (Figure 2d−f) was achieved. It can be seen that two sets of {10} fringe 2d-hexagonal mesostructures have been observed in the samples synthesized with (*R*)-(+)-APP/SDS molar ratios of 0.2 and 0.4, indicating that the chiral structure has

(17) (a) Che, S.; Liu, Z.; Ohsuna, T.; Sakamoto, K.; Terasaki, O.; Tatsumi, T. *Nature* **2004**, *429*, 281. (b) Ohsuna, T.; Liu, Z.; Che, S.; Terasaki, O. *Small1* **2005**, *2*, 233. (c) Jin, H.; Liu, Z.; Ohsuna, T.; Terasaki, O.; Inoue, Y.; Sakamoto, K.; Nakanishi, T.; Ariga, K. Che, S. *Adv. Mater.* **2006**, *18*, 593.
(18) Wu, X.; Jin, H.; Liu, Z.; Ohsuna, T.; Terasaki, O.; Sakamoto, K.; Che, S. *Chem. Mater.* **2006**, *18*, 241.
(19) (a) Dörfler, HD. *Adv. Colloid Interface Sci.* **2002**, *98*, 285.; (b) Eelkema, R.; Feringa, B. L. *J. Am. Chem. Soc.* **2005**, *127*, 13480.
(20) Wang, B.; Chi, C.; Shan, W.; Zhang, Y.; Ren, N.; Yang, W.; Tang, Y. *Angew. Chem., Int. Ed.* **2006**, *45*, 2088.

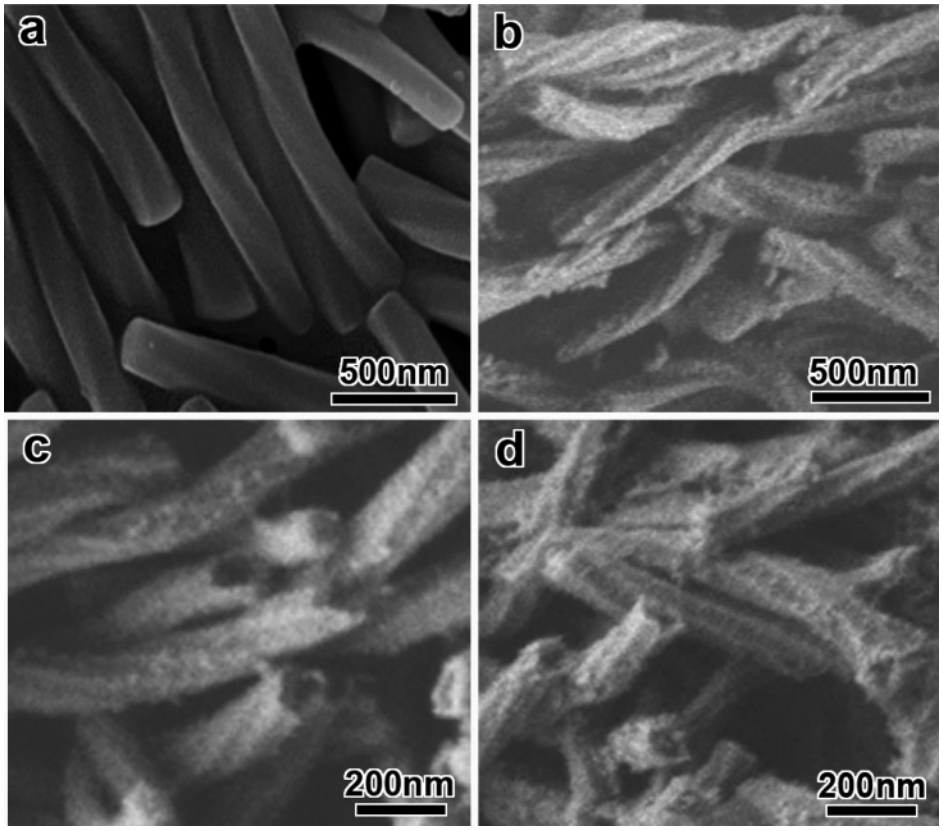


**Figure 1.** SEM images of the calcined samples synthesized with different (*R*)-(+)-APP/SDS molar ratios of (a) 0, (b) 0.2, (c) 0.4, and (d) 0.8. These materials have been synthesized at 30 °C for 6 h and were then allowed to age for 1 day at 90 °C.

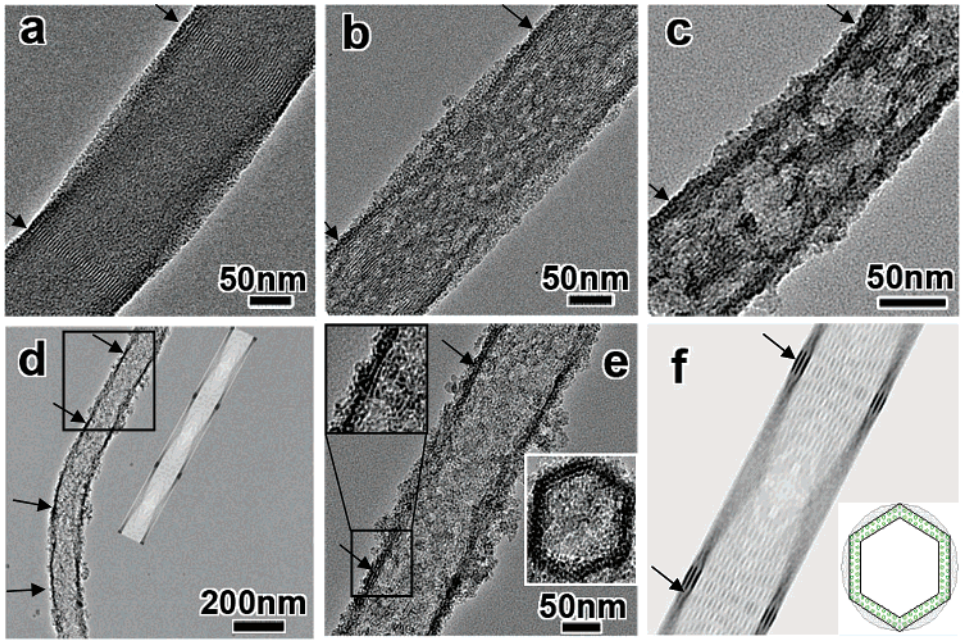


**Figure 2.** (a−c) TEM images of calcined samples shown in Figure 1a−c; (d) low- and (e, f) high-magnification TEM image with simulated chiral nanotubes shown in Figure 1d.

retained even after the formation of macrohollows with sizes ranging from ∼10 to ∼50 nm, which are the meso-macroporous bimodal chiral materials. The presence of the 2d-hexagonal channel structure has also been confirmed by XRD patterns later (Figure 3b). Between two sets of {10} fringes, the tube twists by 60°, which means that the distance between two sets of {10} fringes is one-sixth of one pitch. The helical pitch along the rod axis was estimated to be ∼1.1−1.6 $\mu$m from six distinct surfaces or from the distance between two sets of {10} fringes.

The HRTEM image taken with the incident beam perpendicular to the tube in Figure 2d (also see Figure S1) shows that the whole tube is open-ended, with smooth inner and out surfaces throughout their length. The high-magnification image (Figure 2e) of the area in Figure 2d indicated by rectangular clearly exhibits the fringes on the edge of the

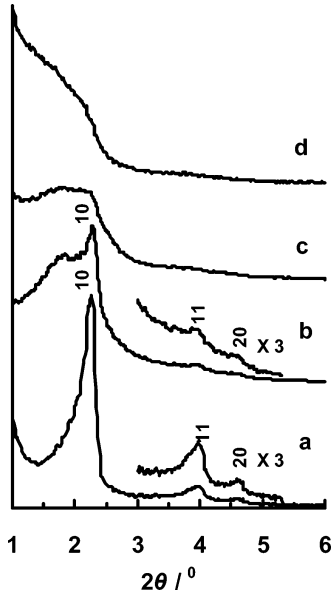


**Figure 3.** XRD patterns of calcined samples shown in Figure 1.

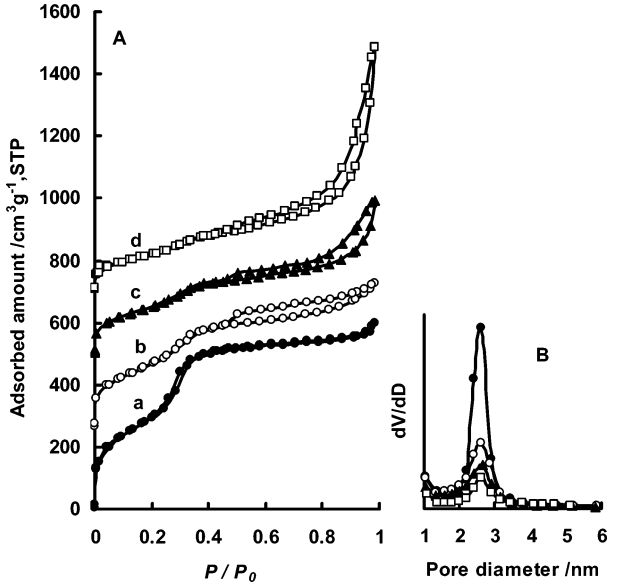


**Figure 4.** $N_2$ adsorption−desorption isotherms and pore size distributions of samples shown in Figure 1.

tube, which correspond to the interplanar space of {10} of the 2d-hexagonal mesostructure. The enlarged image of the nanotube edge was inset in the upper left corner of Figure 2e to further reveal the fine structure. Meanwhile, to confirm the observed image above, the image taken with the incident beam parallel to the tube was also inset at the bottom right of Figure 2e, which distinctly shows the ordered two-layer arranged mesopores in the wall of the tube. To further probe the mesoporous structure of this chiral nanotube material, we simulated the TEM images along both directions by using a specially developed software by TO (Figure 2f). It can be seen that the simulated images fit the TEM images very well, although it is very difficult to unambiguously determine whether the channels are chiral directly from the TEM images. The simulated images imply that these two-layer channels in the tube wall run around the central axis of the rod. It is worth noting that two-layer fringes in the TEM image, indicated by arrows, correspond to the interplanar space (10), as shown in the simulated image.

As reported previously,[17,18,20] the XRD pattern of the sample synthesized without any addition of dopant also showed three peaks (Figure 3), which can be indexed by 10, 11, and 20 reflections on the basis of the hexagonal system with a $d_{10}$ spacing of 3.91 nm. With increasing (*R*)-(+)-APP/surfactant molar ratio from 0.2 to 0.8, the intensity of all peaks was decreased; finally, no resolved peak remained in the XRD patterns, mostly because of the formation of hollow and mesoporous silica nanotubes from the solid to tube.

The structural change due to the addition of (*R*)-(+)-APP has also been confirmed by $N_2$ adsorption−desorption analysis. The nitrogen adsorption−desorption isotherm of the sample synthesized without chiral dopant shows type IV features with only one capillary condensation step at ∼0.4 in relative pressure, which confirmed the existence of uniform mesopores. The isotherms of the samples synthesized with different amounts of (*R*)-(+)-APP addition show two sharp capillary condensation steps in the relative pressure range of 0.4−1.0. The capillary condensation step at ∼0.4 in relative pressure is an indication of typical uniform mesopores in the wall and, consequently, narrow mesopore size distributions (Figure 4B), whereas the capillary condensation step occurring in the relative pressure range of 0.5−0.95 is probably attributed to the nitrogen adsorption in the cavities of the macropores and tubes, which increased with an increasing amount of (*R*)-(+)-APP addition. The pore size distribution also confirmed that the pore volume corresponding to the uniform mesopores decreased with increasing macropore volume. The uniform mesopores with a BJH (Barrett−Joyner−Halenda) pore diameter was about 2.6 nm; the BET (Brunauer−Emmett−Teller) surface area decreased from 1079 $m^2\ g^{-1}$ to 439 $m^2\ g^{-1}$ and mesopore volume decreased from 337 $mm^3\ g^{-1}$ to 115 $mm^3\ g^{-1}$, respectively. The decreasing surface area of the mesoporous tube may be caused by the presence of amorphous silica particles moving outward from the inner during tube formation (discussed further later in this paper).

Overall handedness of this chiral mesoporous silica tube was estimated by counting characteristic morphologies from 500 randomly chosen crystals in the SEM images, and the enatiomeric excess ee (ee $=\{(L - R)/(L + R)\})\times 100\%$, where *L* and *R* are the number of left- and right-handed rods) values were proven to be in increasing order of −11, −19, −25, and −32% for the samples synthesized with increasing (*R*)-(+)-APP/SDS molar ratios of 0.2, 0.4, 0.6, and 0.8, respectively. As expected, enantiomeric dopant (*S*)-(−)-APP gave the mirror-imaged profiles; all of the helical mesoporous silicas synthesized with different (*S*)-(−)-APP/SDS molar ratio were similar to those of the (*R*)-(+)-APP dopant system. In our previous work, it has been found that the left-/right-handedness ratio 1:1 of helical mesoporous silica formed from achiral surfactant SDS assembly.[18] The small chiral molecules play an important role in obtaining chiral sense of the excess mesoporous materials, but only a limited ee value can be obtained by adding chiral dopant, which is quite different from the traditional understandings of helical lyotropic liquid crystal.

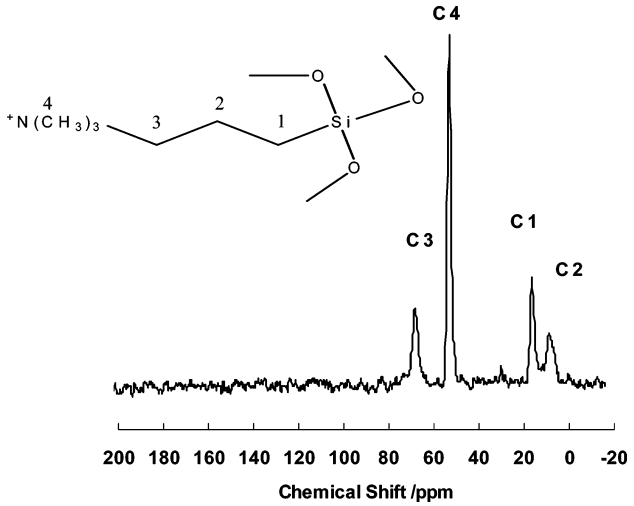


**Figure 5.** $^{13}C$ CP/MAS NMR spectrum of extracted mesoporous silica nanotubes.

The quaternary amine group functionalized mesoporous silica nanotubes have been obtained by removing surfactant. $^{13}C$ CP/MAS NMR spectrum (Figure 5) has confirmed that the surfactant molecules were entirely removed after extraction. No resonance signal was detected between 20 and 40 ppm, which is attributed to the alkyl of SDS, and the resonance signals at 8.11, 16.76, 53.19, and 68.26 ppm should be assigned to C2, C1, C4, and C3 of TMAPS, respectively. These demonstrated that the SDS molecules and APP were removed and that the quaternary amine groups stayed on the mesopores surface. Elemental analysis results showed that carbon contained in the material is attributed to the hydrolysis and co-condensation of TMAPS and TEOS, and the loading amount of organic groups $(-CH_2)_3N^+(CH_3)_3$ is 1.16 mmol/g $SiO_2$.

**2. Time Course of Tube Formation.** To investigate the structural evolution of the chiral mesoporous silica tube with synthesis time, XRD patterns (Figure 6), SEM (Figure 7), and HRTEM images (Figure 8) of the products at an 0.8 (*R*)-(+)-APP/SDS molar ratio were obtained as a function of the reaction time. The XRD peaks were broadened with reaction time and finally no peaks appeared.

The material was kept at 30 °C and sampled every 30 min for 5 h. The material taken after 30 min showed the nice twisted hexagonal rod morphology (Figure 7a), but the internal structure was not observed (Figure 8a); the 2d-hexagonal twisted mesostructure was formed at 2 h and maintained to 5 h (Figurse 6b, 7b, and 8b) while maintaining the morphology. No structural change was observed after 4 h at 30 °C. However, the material was placed after forming the 2d-hexagonal twisted mesostructure at 90 °C, and the hollow started forming after 1 h (not shown). The material was gradually transformed from a solid with chiral mesoporous structure[17] (images a and b of Figure 8) to a hollow rod (Figure 8c) and finally to a tube (Figure 8d), which was consistent with the XRD observations. The pure mesoporous silica nanotubes have been observed from the samples aged for even 3 days. The small amorphous particles appeared at an external surface of the tube obtained after 1 h at 90 °C and may be formed from the inner part of the solid rod by hollowing it out. The particles can be observed from the SEM

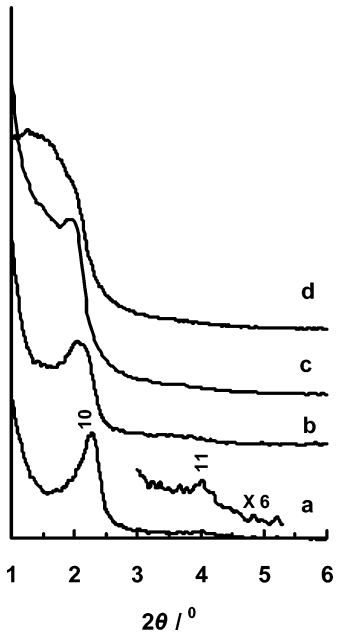


**Figure 6.** XRD patterns of as-synthesized chiral nanotubes sampled at different reaction times from the chiral mesoporous silica nanotubes formation system ((*R*)-(+)-APP/SDS = 0.8) at (a) 30 °C for 30 min, (b) 30 °C for 5 h, (c) 90 °C for 8 h, and (d) 90 °C for 14 h.

images (images c and d of Figure 7) synthesized at 90 °C for 8 and 14 h. It has been found that the hollows in the chiral tube have never been formed when the temperature of the synthesis gel was kept at 30 °C even for 4 days. Tubular structures have not been found in the synthesis systems with APP/SDS molar ratios of 0.2−0.4 for longer reaction times.

The novel route proceeds by hollowing out of the chiral mesoporous silica and maintaining a constant helical width. This mechanism is quite different from that observed for the supramolecular templates,[13] helical ribbon turning route,[14] and the formation in a physically confined environment.[16] Typically, it has been considered that rod-shaped molecular assemblies can produce tubular morphologies, or the morphology of a helical fiber could turn out to be helical tubes, respectively. It is conceivable that the incipient chiral mesoporous crystallization is responsible for the formation of the hollow tubular morphologies. A possible mechanism might involve, at the early stages, the SDS surfactant, (*R*)-(+)-APP, and silica source TEOS being self-assembled to form a well-defined chiral liquid crystal and subsequent hydrolysis−condensation of the silica precursor being performed at the surface of the surfactant. Perhaps the formation mechanisms for tubular structures are related to the different density or composite between the surface and inside of the chiral rod. With increasing temperature, the outer wall of the rod would be condensed with the reaction time because of the contact with the synthesis gel solution, and the inside of the rod would be dissolved because of the large amount of organics and incompletely condensed silica wall.

**3. Synthesis of Mesoporous Silica with Different Dopants Additions.** To understand the formation mechanism of the chiral silica nanotube with a hollow induced by dopants, a series of designed dopants were incorporated into the system to recognize the importance of functional groups of APP.

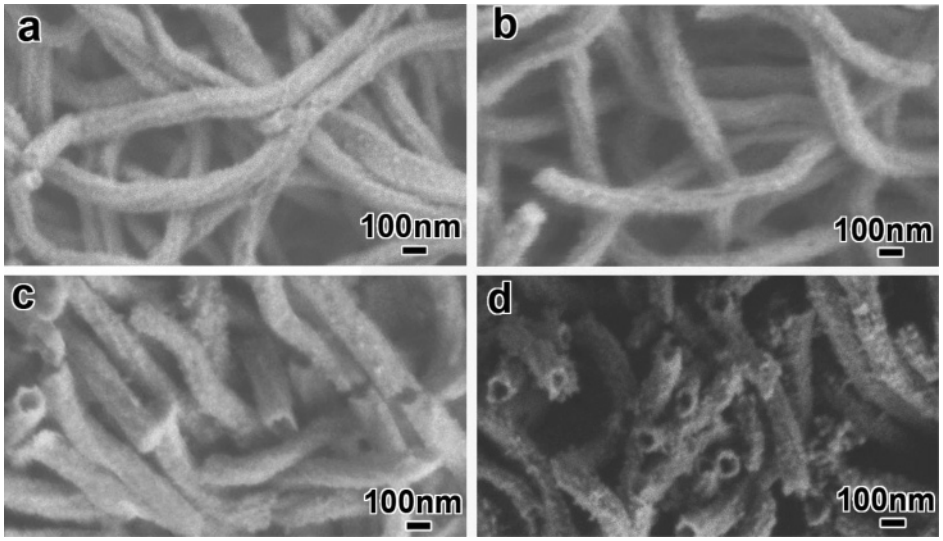


**Figure 7.** SEM images of the as-synthesized samples shown in Figure 6.

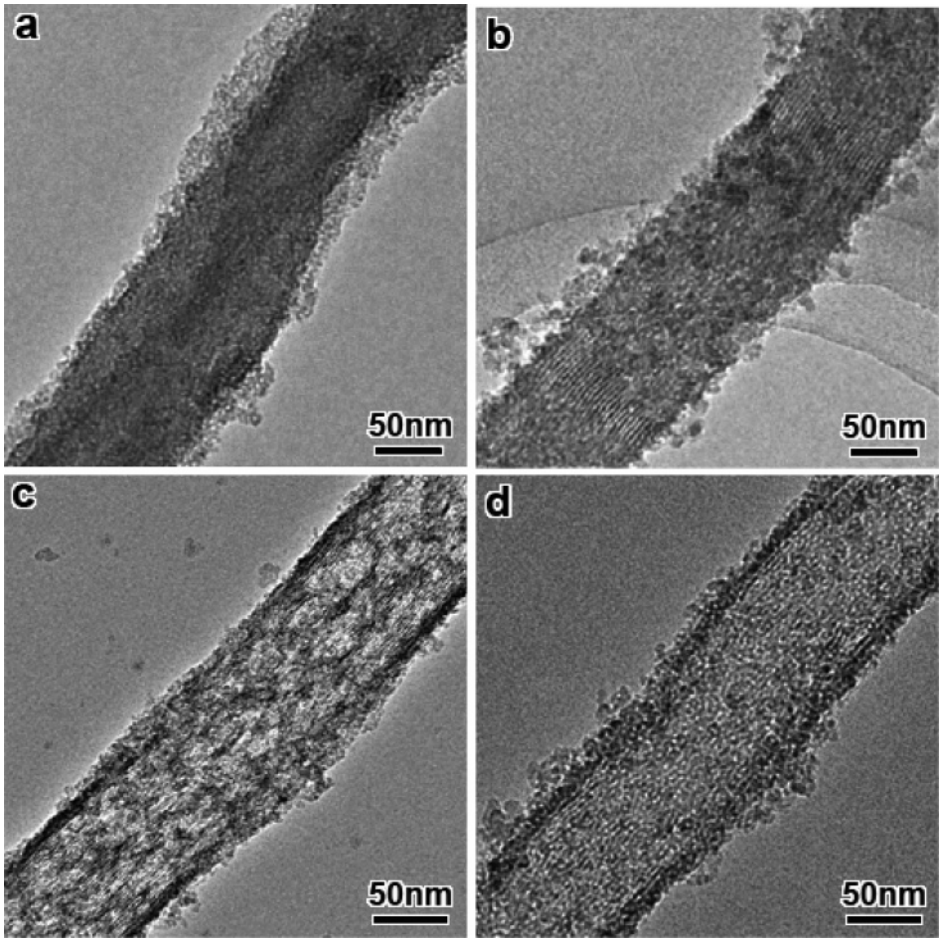


**Figure 8.** TEM images of the as-synthesized samples shown in Figure 6.

The synthesis behaviors with the addition of various aromatic hydrocarbons, alcohols with different chain lengths, and amines have been examined. The TEM images of a representative sample synthesized by adding different dopants with different functional groups are shown in Figure 9. It can be seen that the existence of the amino group determines the formation of nanotube, whereas the use of various hydrocarbons and alcohols resulted in the chiral mesoporous silica without hollow or irregular shapes when the amount of dopant is increased (not shown). We propose, therefore, that the addition of amine plays an important role in the mechanism of silica tube formation because it is the strong basic nature that leads to highly charged anionic silicate species in solution and a lower rate of condensation,[21] causing soft, soluble walls of the solid mesoporous chiral rod. When the amino acids such as L-troptophone, L-alanine, L-valine,

(21) *The Chemistry of Silica*; Iler, R. K., Ed.; Wiley: New York, 1979.

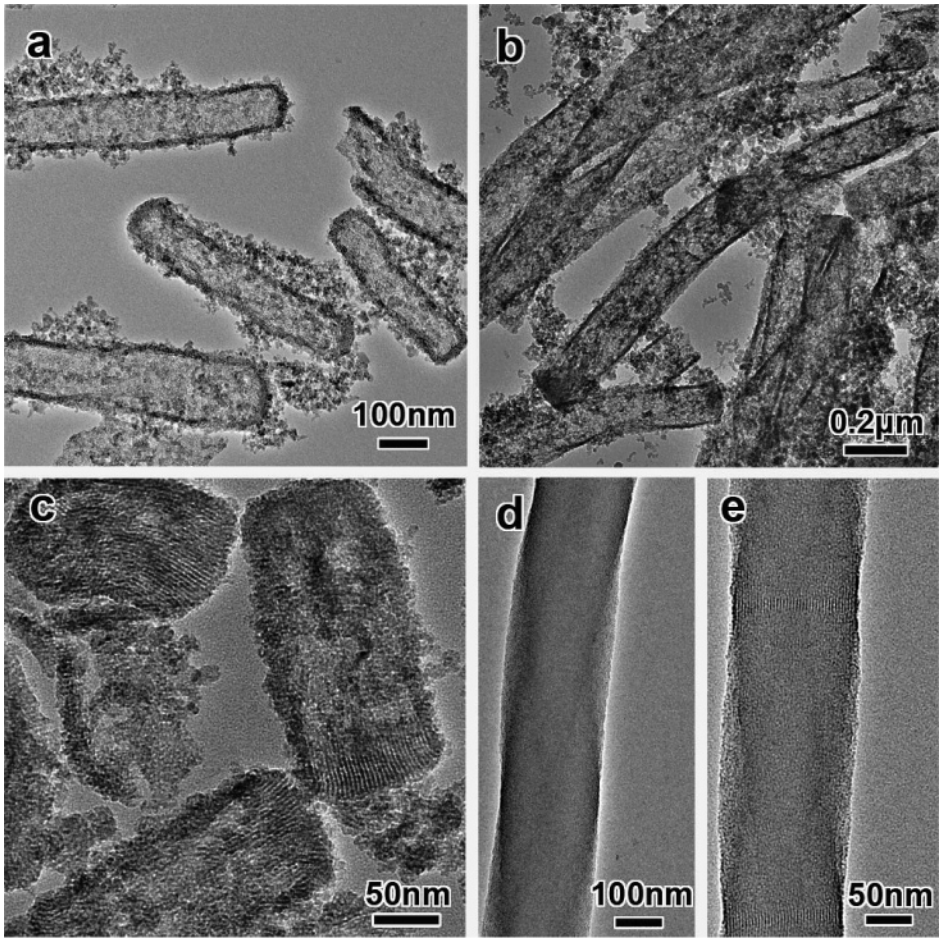


**Figure 9.** TEM images of the calcined samples synthesized by adding different dopants: (a) L-alaninol/SDS = 0.3, (b) *n*-propylamine/SDS = 0.3, (c) ethanol amine/SDS = 0.3, (d) propanol/SDS = 0.6, and (e) *n*-hexane/SDS = 0.6.

L-phenylalanine, and *N*-acetyl-L-phenylalanine were added as dopant, the chiral mesostructure was formed only with a molar ratio of amino acid/SDS < 0.2, and the products were similar in the morphology and chirality of the sample formed without the dopant. The ineffectiveness of the amino acids on the formation of the mesoporous silica tube would be due to their relatively low basicity. However, it is not very clear at present which one is the main factor in deciding the mechanism of tube formation.

## Conclusions

To the best of our knowledge, this is the first synthesis of silica nanotubes with chiral mesoporous wall by using organic surfactant as template in the presence of chiral dopant. The co-associated properties of the organic additives and chiral molecules play an important role for the formation of tube shape and handedness excess, respectively. Interestingly, the mesoporous silica nanotubes have been produced through a specific crystallization route that hollows out the chiral mesoporous silica rod. The incorporation of a chiral channel with a quaternary amine group in the walls of the tubular silica may lead to materials with interesting properties and provide a new insight into the molecular factors governing inorganic−organic macro- and mesophase formation. On the other hand, this novel material is also very promising for gas storage, catalyst, or catalyst supports.

**Acknowledgment.** This work was supported by the National Natural Science Foundation of China (Grants 20425102 and 20521140450), the China Ministry of Education and the Shanghai Science Foundation (0452nm061 and 05XD14010). O.T. thanks the Swedish Science Research Council (VR) and the Japan Science and Technology Agency (JST) for financial support. The authors are grateful to Instrumental Analysis Center, Shanghai Jiao Tong University, for taking elemental analysis.

**Supporting Information Available:** Low-magnification HRTEM images of the samples shown in Figure 2. This material is available free of charge via the Internet at http://pubs.acs.org.

CM062368M